Exact Box-constrained Economic Operating Region for Power Grids Considering Renewable Energy Sources

Huating Xu, Bin Feng, Chutong Wang, Chuangxin Guo, Jian Qiu, and Mingyang Sun

***Abstract*—The growing integration of renewable energy generation manifests as an effective strategy for reducing carbon emissions. This paper strives to efficiently approximate the set of optimal scheduling plans (OSPs) to enhance the performance of the steady-state adaptive cruise method (SACM) of power grid, improving the ability of dealing with operational uncertainties. Initially, we provide a mathematical definition of the exact box-constrained economic operating region (EBC-EOR) for the power grid and its dispatchable components. Following this, we introduce an EBC-EOR formulation algorithm and the corresponding bi-level optimization models designed to explore the economic operating boundaries. In addition, we propose an enhanced big-*M* method to expedite the computation of the EBC-EOR. Finally, the effectiveness of the EBC-EOR formulation, its economic attributes, correlation with the scheduling plan underpinned by model predictive control, and the significant improvement in computational efficiency (over twelvefold) are verified through case studies conducted on two test systems..**

***Index Terms*—Exact box-constrained economic operating region (EBC-EOR), big-*M* method, intelligent scheduling, steady-state adaptive cruise, uncertainty, renewable energy source.**

NOMENCLATURE

A. Indices and Sets

τ	Constraint index of optimization model
$\Psi_{i,t}^{BC,com}$	Exact box-constrained economic operating region (EBC-EOR) of power grid components
$\Psi_{t}^{BC,gri}$	EBC-EOR of power grid
i	Index of dispatchable components or generators
j	Index of wind power generation
k	Index of wind power generation scenarios
l	Index of transmission lines
min, max	The minimum and maximum values
r	Index of load
S_t	Economic operating region of power grid
t	Time step index
U_t	Uncertainty set of $\boldsymbol{u}_t$

B. Parameters and Constants

$\pi_{l,i}^{G}$, $\pi_{l,j}^{W}$, $\pi_{l,r}^{D}$	Power transfer distribution factors of generators, wind farms, and loads
a_i, b_i, c_i	Cost coefficients of generators
$f_l^{\max}$	Transmission capacity of tie lines
H	Time period of model predictive control
M	A large enough constant
M_τ	Individually evaluated M value for the τ^{th} constraint
m_1, m_2, m_3	Preset parameters for enhanced big-M method
N_G, N_W, N_D	Number of dispatchable generators, wind farms, and loads
N_T, N_S	Number of scheduling time periods and wind power generation scenarios
$p_{r,t}^{D}$	Demand of load r at time step t
$p_i^{G,\min}, p_i^{G,\max}$	The minimum and maximum active power outputs of generator i
RD_i, RU_i	Ramp-rate limits of generator i
$\underline{W}_{j,t}, \overline{W}_{j,t}$	The lower and upper bounds of wind generation j at time step t
$\mathbf{1}$	Column vector whose elements are all equal to 1

C. Variables and Optimization Models

$\boldsymbol{\theta}$	Vector of binary variables, $\boldsymbol{\theta}=[\theta_\tau]$, $\forall\tau$
$\boldsymbol{\lambda}$	Vector of dual variables, $\boldsymbol{\lambda}=[\lambda_\tau]$, $\forall\tau$
diag($\boldsymbol{\lambda}$)	Diagonal matrix whose diagonal elements are $\boldsymbol{\lambda}$
$\boldsymbol{f}_t$	Basic optimal scheduling model corresponding to $\boldsymbol{u}_t$
$\boldsymbol{P}_G$	Vector of active power output of generators, $\boldsymbol{P}_G=[p_{i,t}^{G}]$, $\forall i, \forall t$
p_t^{gri}	Total power generation of power grid
$\boldsymbol{P}_W$	Vector of wind power generation, $\boldsymbol{P}_W=[p_{j,t}^{W}]$,

Manuscript received: May 15, 2023; revised: June 18, 2023; accepted: July 6, 2023. Date of CrossCheck: July 6, 2023. Date of online publication: September 1, 2023.

This work was supported by the Science and Technology Project of State Grid Corporation (No. 5400-202099286A-0-0-00).

This article is distributed under the terms of the Creative Commons Attribution 4.0 International License (http://creativecommons.org/licenses/by/4.0/).

H. Xu, B. Feng, C. Wang, C. Guo (corresponding author), and J. Qiu are with the College of Electrical Engineering, Zhejiang University, Hangzhou 310027, China (e-mail: xu_huating@zju. edu. cn; fengbinhz@zju. edu. cn; wangchutong94@foxmail.com; guochuangxin@zju.edu.cn, jianqiu@zju.edu.cn).

M. Sun is with the Department of Control Science and Engineering, Zhejiang University, Hangzhou 310027, China (e-mail: mingyangsun@zju.edu.cn).

DOI: 10.35833/MPCE.2023.000312

	$\forall j, \forall t$
$\boldsymbol{P}_{W,cur}$	Vector of wind power curtailment, $\boldsymbol{P}_{W,cur}=[p_{j,t}^{W,cur}]$, $\forall j,\forall t$
$\boldsymbol{u}_t$	Vector of uncertainty variables of power grid
$\boldsymbol{x}_t$	Vector of optimal output of a power grid dispatchable component, $\boldsymbol{x}_t=[x_{i,t}]$, $\forall i$

I. Introduction

In recent years, the pursuit of a cleaner, low-carbon, and sustainable future energy system [1]-[3] has resulted in a significant increase in the proportion of power generated by renewable energy sources (RESs) [4]. However, unlike traditional generators (which provide better regulation performances) and conventional loads (which can be forecasted with higher accuracy), the RES output is highly variable and challenging to forecast with high precision [5]. In order to ensure the safe operation of the power grid, the dispatchers often develop day-ahead scheduling plans based on conservative estimates of RES outputs, which makes it challenging to track the optimal operating point of power grid in real time. As a result, the curtailment of RESs frequently transpires [6].

Researchers engaged in power grid dispatching have investigated a variety of strategies to mitigate RES curtailment [7]-[11]. During the day-ahead stage, numerous methods including two-stage robust optimization [7], two-stage stochastic optimization [9], distributionally robust optimization [11], multi-stage robust optimization [12], among others, are studied. These aim to deliver a robust and cost-effective day-ahead scheduling plan for the power grid, equipped to manage any unforeseen RES generation that might arise within the subsequent scheduling cycle. Nonetheless, these methods often produce day-ahead scheduling plans optimized for specific extreme scenarios, consequently becoming overly conservative for the majority of conventional operational conditions. During the intra-day stage, with the intention of adapting to the rapid fluctuations in the optimal operating point of power grid due to RES integration, [13] and [14] implement offline training and online application strategies to provide near-real-time scheduling plans. However, the extensive nature of the action space that must be explored makes the training process time-intensive.

The traditional scheduling plan, deduced via the above-mentioned methods, fundamentally serves as a base operating point. It only provides localized operational information for a power grid under uncertainties, rendering it arduous to accurately track the optimal operating point of power grid. In order to augment the economic operation of the power grid and enhance the accommodation of RESs, alterations in future power grid characteristics and new dispatching technology requirements are meticulously analyzed in [15] and [16]. Following this, [17] and [18] introduce the steady-state adaptive cruise method (SACM) for future intelligent dispatching, which is encapsulated in two primary stages. Initially, in the offline stage, the uncertainties in the power grid are predicted, and a corresponding set of optimal scheduling plans (OSPs) for a predefined future timescale is crafted. This stage contributes global (not merely localized) operational information for the power grid. Subsequently, in the online stage, an appropriate OSP is swiftly selected from the pre-formulated set, facilitating intelligent real-time dispatch of the power grid (i.e., from the global operational information of power grid back to the optimal local operational information). This sequence enables the power grid to nimbly follow the optimal operating point with elevated temporal resolution.

Extensive research has been undertaken to delineate the operating region of the power grid (i.e., the set of feasible operating points). Studies like [5] and [6] focus on formulating the dispatchable region of wind power generation. These investigations, however, primarily outline the wind power generation accommodation boundary and neglect the set of dispatching plans. In [19]-[26], security regions are crafted for distribution systems, integrated energy systems, tie lines, among others. The principal focus of these security regions, though, lies on the security of the power grid, with scant attention paid to economic factors. As a result, most scheduling plans within the security region fail to qualify as OSPs. Taking economics into account, [27] computes the set of OSPs for multi-objective dispatching preferences. Regrettably, this approach merely reserves a fixed capacity to mitigate operational uncertainty, thus failing to provide global operational information for the power grid. References [28] and [29] propose delineating the operating region using box constraints of power grid, yet it still fails to encompass all OSPs under uncertainties due to the requisite that all boundary operating points adhere to the ramp-rate limits of generators. Reference [30] mathematically defines the set of OSPs under uncertainties as the economic operating region (EOR) of power grid, proposing a bi-level iteration method to calculate the convex hull of the power grid EOR, factoring in RES uncertainty. However, this method bears two primary shortcomings. Firstly, as the number of dispatchable generators escalates, so does the number of the convex hull vertices that require individual calculation, leading to a significant computational burden. Secondly, when the generator count surpasses three, it relies on dimension reduction technology to visualize the convex hull of EOR.

This paper aims to address the economic and computational complexity challenges in [28]-[30]. We propose the definition and formulation of an exact box-constrained economic operating region (EBC-EOR), along with a relevant solution method. The key contributions of our study are highlighted as follows.

1) To thoroughly encompass the OSPs under uncertainties and provide global operational information, the easy-to-visualize EBC-EOR is mathematically defined for the power grid and its dispatchable components.

2) Bi-level optimization models and a progressive boundary-searching algorithm are proposed to determine the EBC-EOR.

3) An acceleration strategy (enhanced big-*M* method) is proposed to refine the traditional big-*M* method, which facilitates an increase of more than twelvefold in the computation-

al efficiency of the EBC-EOR.

The rest of this paper is structured as follows. In Section II, we present a brief introduction to the SACM, the mathematical definitions of the EBC-EOR, and the bi-level optimization models that relate to the EBC-EOR. Section III delves into the calculation method for the EBC-EOR and the associated acceleration strategy. In Section IV, we present case studies illustrating the visualization, economic implications, connection to model predictive control (MPC), and computational efficiency of the EBC-EOR. We conclude this paper in Section V.

II. Definition and Formulation

A. Brief Introduction of SACM

Figure 1 showcases one of the technical routes to support the SACM, a novel scheduling technique devised to bolster the capacity of power grid to track its optimal operating point under uncertainties and reduce RES curtailment [16], [17]. The SACM, operationalized on the scheduling platform, comprises two stages − offline and online. It supervises the operating state of power grid and dispatches the power grid flexibly and intelligently. In the offline stage, uncertainty sets pertaining to RESs, loads, and other variables are predicted for the power grid. Then, the multi-period EOR of power grid for the forthcoming scheduling cycle is periodically calculated, grounded in these uncertainty sets. The EOR encompasses the global economic operational information (a collection of all the OSPs under uncertainties) of power grid. This contrasts with the local economic operational information rendered by the conventional single OSP. In the online stage, the OSP from the EOR is swiftly matched and evaluated based on real-time loads and RES generation. According to the evaluation outcomes, power grid dispatchers have the latitude to modify the scheduling objective of EOR. Finally, the real-time scheduling of power grid is executed based on the matched OSP and source-load cooperative control [18].

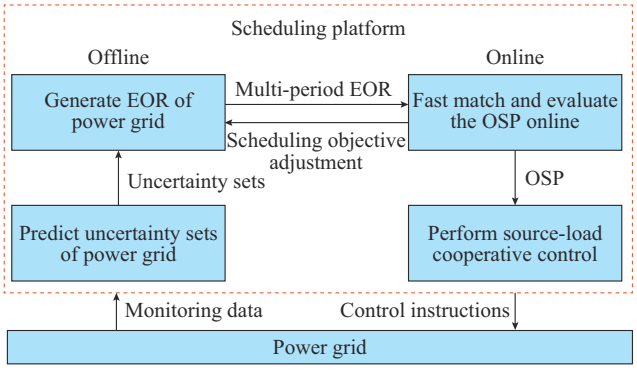

Fig. 1. Brief flow chart of SACM.

B. Definition of Proposed EBC-EOR

1) EOR

In [30], the EOR of power grid is defined as:

$$S_t=\{\boldsymbol{x}_t|\boldsymbol{x}_t=\boldsymbol{f}_t(\boldsymbol{u}_t),\forall\boldsymbol{u}_t\in\boldsymbol{U}_t\} \tag{1}$$

where $\boldsymbol{u}_t$ can be either continuous or discrete, representing any uncertainties of the power grid including RES generation, load demand, equipment outage, natural disasters, human factor risk, etc.; the objective of $\boldsymbol{f}_t$ can be a single- or multi-combination of the lowest operating cost, the lowest carbon emission, and the lowest operating risk, etc.; and $\boldsymbol{x}_t$ is essentially the OSP of dispatchable components [30]. EOR is essentially the set of OSPs of power grid under uncertainties.

2) EBC-EOR

Usually, S_t is a nonconvex set [30] that is notoriously hard to handle. To trade off the computational complexity, engineering practicality, and economic problems in [28]-[30], we propose to formulate the EBC-EOR to approximate the exact EOR. Essentially, the EBC-EOR provides a box-type coverage of an OSP set, outlining the potential range of the OSP set. For the convenience of dispatchers, we define the EBC-EORs of dispatchable components and the power grid as follows.

1) Definition 1: the EBC-EOR of dispatchable component i at time step t is defined as $\Psi_{i,t}^{BC,com}=\{x_{i,t}|\,x_{i,t}^{\min}\le x_{i,t}\le x_{i,t}^{\max}\}$, where $x_{i,t}^{\min}=\min\limits_{\boldsymbol{x}_t\in S_t}x_{i,t}$, and $x_{i,t}^{\max}=\max\limits_{\boldsymbol{x}_t\in S_t}x_{i,t}$.

2) Definition 2: the EBC-EOR of the power grid at time step t is defined as $\Psi_t^{BC,gri}=\{p_t^{gri}|\,p_t^{gri,\min}\le p_t^{gri}\le p_t^{gri,\max}\}$, where $p_t^{gri,\min}=\min\limits_{\boldsymbol{x}_t\in S_t}\boldsymbol{1}^{\mathrm{T}}\boldsymbol{x}_t$, and $p_t^{gri,\max}=\max\limits_{\boldsymbol{x}_t\in S_t}\boldsymbol{1}^{\mathrm{T}}\boldsymbol{x}_t$.

It should be noted that, in this paper, the EBC-EOR of power grid is exclusively associated with the range of total active power output (i.e., $\boldsymbol{x}_t$ in Definition 2 is confined to the active power of dispatchable components). Definition 1 and Definition 2 clarify that the remaining task in formulating the EBC-EORs of dispatchable components and power grid involves determining $x_{i,t}^{\min}$, $x_{i,t}^{\max}$, $p_t^{gri,\min}$, and $p_t^{gri,\max}$.

C. Basic Optimal Scheduling Model

As outlined in Section II-B, the EBC-EOR relates to the uncertainty set U_t (represented by box constraints in Section II-D) and the basic optimal scheduling model (OSM) $\boldsymbol{f}_t$. In this study, we investigate the EBC-EOR under wind power generation uncertainty. Here, the dispatchable components solely comprise generators, with the unit commitment presumed to be known. The corresponding basic OSM, which seeks to maximize the wind power accommodation at the minimum cost, is formulated as:

$$\min\sum_{t=1}^{N_T}\sum_{i=1}^{N_G}(a_i(p_{i,t}^G)^2+b_ip_{i,t}^G+c_i) \tag{2}$$

s.t.

$$p_i^{G,\min}\le p_{i,t}^G\le p_i^{G,\max}\quad\forall i,\forall t \tag{3}$$

$$-RD_i\le p_{i,t+1}^G-p_{i,t}^G\le RU_i\quad\forall i,\forall t \tag{4}$$

$$0\le p_{j,t}^{W,cur}\le p_{j,t}^W\quad\forall j,\forall t \tag{5}$$

$$-f_l^{\max}\le\sum_{i=1}^{N_G}\pi_{l,i}^Gp_{i,t}^G+\sum_{j=1}^{N_W}\pi_{l,j}^W(p_{j,t}^W-p_{j,t}^{W,cur})-\sum_{r=1}^{N_D}\pi_{l,r}^Dp_{r,t}^D\le f_l^{\max}\quad\forall l,\forall t \tag{6}$$

$$\sum_{i=1}^{N_G}p_{i,t}^G+\sum_{j=1}^{N_W}(p_{j,t}^W-p_{j,t}^{W,cur})-\sum_{r=1}^{N_D}p_{r,t}^D=0\quad\forall t \tag{7}$$

Constraint (3) limits the output range of generators. Constraint (4) defines the ramp limit of generators. Constraint (5) denotes the range of wind curtailment. Constraint (6) limits the transmission capacity of line power flow based on the power transfer distribution factors [5], [6]. Constraint (7) is the power balance condition. The basic OSM is constructed based on a DC power flow model, which is widely accepted in economic dispatching problems [31]. For the convenience of the subsequent expression, we write the compact form, which is a common representation [6], [31], [32], of (2)-(7) as:

$$\min(\boldsymbol{P}_G^{\mathrm{T}}\boldsymbol{A}\boldsymbol{P}_G+\boldsymbol{B}^{\mathrm{T}}\boldsymbol{P}_G+\mathbf{1}^{\mathrm{T}}\boldsymbol{C}) \tag{8}$$

s.t.

$$\boldsymbol{E}\boldsymbol{P}_G+\boldsymbol{F}\boldsymbol{P}_W+\boldsymbol{K}\boldsymbol{P}_{W,cur}+\boldsymbol{G}\le\mathbf{0} \tag{9}$$

where matrices $\boldsymbol{A},\boldsymbol{E},\boldsymbol{F},\boldsymbol{K}$ and vectors $\boldsymbol{B},\boldsymbol{C},\boldsymbol{G}$ correspond to the coefficients in (2)-(7). The formulation of coefficient matrices and vectors is shown in Appendix A.

The basic OSM determines the scheduling objective of EOR. It can be designed and modified according to the requirements of grid dispatchers (introduced in Section II-A). Thus, the EBC-EOR can also be explored based on other basic OSMs, even containing energy storage [33].

D. Searching Boundary of EBC-EOR

To delineate the boundaries of the EBC-EOR, we formulate the bi-level optimization problems (10)-(12) and (13)-(15), pertaining to the EBC-EOR of generator and the EBC-EOR of power grid, respectively.

$$\min(\max)\, p_{i,t}^{G} \tag{10}$$

s.t.

$$\underline{W}_{j,t}\le p_{j,t}^{W}\le \overline{W}_{j,t}\quad \forall j,\forall t \tag{11}$$

$$[\boldsymbol{P}_G]\in \arg\{(8),\text{s.t. }(9)\} \tag{12}$$

$$\min(\max)\, p_{t}^{gri} \tag{13}$$

s.t.

$$p_t^{gri}=\sum_{i=1}^{N_G} p_{i,t}^{G} \tag{14}$$

$$(11),\ (12) \tag{15}$$

The operator "min(max)" in (10) and (13) means solving the minimum (maximum) values of objective function, which are equivalent to two independent optimization problems for searching the lower and upper boundaries of EBC-EOR (i.e., (10)-(12) and (13)-(15) represent four independent optimization models); box constraint (11) represents the wind power generation uncertainty range and is embedded in the upper-level optimization; and constraint (12) guarantees $P_{i,t}^{G}$ in the EOR of each time step.

By solving (10)-(12), we can derive the minimum $p_{i,t}^{opt,\min}$ and maximum $p_{i,t}^{opt,\max}$ output power of generators in the EOR. Analogously, the minimum $p_t^{gri,\min}$ and maximum $p_t^{gri,\max}$ output power of power grid in the EOR can be procured by solving (13)-(15).

Since this paper primarily centers on the definition and calculation of the EBC-EOR, uncertainty set prediction is not our main research focus. Consequently, we apply typical box constraints to depict wind power generation uncertainty [34]. The uncertainty set may be altered to other convex forms [31], preserving the identical compact form and solution process. Exploring the calculation of the EBC-EOR based on various types of uncertainty sets forms part of the future research agenda.

III. Methodology

A. Overall Algorithm

This subsection presents the overall process for calculating the EBC-EOR, as shown in Algorithm 1. In line 1, the EBC-EOR of generator $\Psi_{i,t}^{BC,gen}$ and the EBC-EOR of power grid $\Psi_t^{BC,gri}$ are initialized as empty sets. Then, the loops starting from lines 2 and 3 progressively determine the EBC-EORs of generators and power grid. Specifically, in line 4, the upper and lower box boundaries of the EOR of generators are obtained by solving (10)-(12). The EBC-EOR of generators is updated in line 5. Similarly, the upper and lower box boundaries of the EOR of power grid are obtained by solving (13)-(15) in line 7, and the EBC-EOR of power grid is updated in line 8. Finally, when the loops terminate, the EBC-EORs of generators and power grid are output as the sets of $\Psi_{i,t}^{BC,gen}$ and $\Psi_t^{BC,gri}$, respectively.

Algorithm 1: calculating EBC-EOR

Input: total scheduling time steps N_T
Output: $\Psi_{i,t}^{BC,gen}$, $\Psi_t^{BC,gri}$, $\forall t$, $\forall i$
1. Initialize $\Psi_{i,t}^{BC,gen}=\varnothing$, $\Psi_t^{BC,gri}=\varnothing$, $\forall t,\forall i$
2. **for** $t=1{:}N_T$ **do**
3. **for** $i=1{:}N_G$ **do**
4. Solve (10)-(12) to obtain $p_{i,t}^{opt,\min}$ and $p_{i,t}^{opt,\max}$ (which is discussed in Section III-B)
5. Update $\Psi_{i,t}^{BC,gen}=\{p_{i,t}^{G}\,|\,p_{i,t}^{opt,\min}\le p_{i,t}^{G}\le p_{i,t}^{opt,\max}\}$
6. **end**
7. Solve (13)-(15) to obtain $p_t^{gri,\min}$ and $p_t^{gri,\max}$ (which is discussed in Section III-B)
8. Update $\Psi_t^{BC,gri}=\{p_t^{gri}\,|\,p_t^{gri,\min}\le p_t^{gri}\le p_t^{gri,\max}\}$
9. **end**

It is worth mentioning that the bi-level optimization models ((10)-(12) and (13)-(15)) proposed in this paper for EBC-EOR formulation share a conceptual resemblance with the subproblem for generating extreme scenarios in two-stage robust optimization. Despite this similarity, they diverge substantially in their overall algorithm. Typically, the objective functions of the upper-level and lower-level optimization in the subproblem of two-stage robust optimization are identical. In contrast, the objective functions differ in the proposed bi-level optimization models. Moreover, the two-stage robust optimization is typically solved through an iterative procedure between the master problem and subproblem, while Algorithm 1 incrementally establishes the EBC-EOR boundaries by progressively solving a set of independent bi-level optimization problems.

It becomes apparent that all optimization problems ((10)-(12) and (13)-(15)) in Algorithm 1 can be resolved independently. Thus, the proposed algorithm lends itself well to par-

allel computation, which can significantly enhance the computational efficiency.

B. Formulating Single-level Optimization

Since the bi-level optimization problems ((10) - (12) and (13) - (15)) are not straightforward to most of off-the-shelf solvers [5], we propose reformulating their equivalent single-level form.

Firstly, transform (8) and (9) with the corresponding Karush-Kuhn-Tucker (KKT) conditions, which are sufficient and necessary [32].

$$\begin{cases} \boldsymbol{E}\boldsymbol{P}_G + \boldsymbol{F}\boldsymbol{P}_W + \boldsymbol{K}\boldsymbol{P}_{W,cur} + \boldsymbol{G} \le \boldsymbol{0} \\ \boldsymbol{\lambda} \ge \boldsymbol{0} \end{cases} \tag{16}$$

$$\mathrm{diag}(\boldsymbol{\lambda})(\boldsymbol{E}\boldsymbol{P}_G + \boldsymbol{F}\boldsymbol{P}_W + \boldsymbol{K}\boldsymbol{P}_{W,cur} + \boldsymbol{G}) = \boldsymbol{0} \tag{17}$$

$$\begin{cases} 2\boldsymbol{A}\boldsymbol{P}_G + \boldsymbol{B} + \boldsymbol{E}^{\mathrm{T}}\boldsymbol{\lambda} = \boldsymbol{0} \\ \boldsymbol{K}^{\mathrm{T}}\boldsymbol{\lambda} = \boldsymbol{0} \end{cases} \tag{18}$$

Constraint (16) guarantees the primal and dual feasible; constraint (17) is the complementary slackness condition; and constraint (18) represents the stationary condition [32].

Then, linearize the nonconvex and nonlinear constraint (18) with the big-M method [5], shown as:

$$-M\boldsymbol{\theta} \le \boldsymbol{E}\boldsymbol{P}_G + \boldsymbol{F}\boldsymbol{P}_W + \boldsymbol{K}\boldsymbol{P}_{W,cur} + \boldsymbol{G} \le \boldsymbol{0} \tag{19}$$

$$\boldsymbol{0} \le \boldsymbol{\lambda} \le M(\boldsymbol{1} - \boldsymbol{\theta}) \tag{20}$$

Finally, we can rewrite the bi-level optimization problems ((10)-(12), (13) and (15)) in the following equivalent single-level form.

$$\begin{cases} \min(\max)\, p_{i,t}^{G} \\ \text{s.t. (11), (16), (18)-(20)} \end{cases} \tag{21}$$

$$\begin{cases} \min(\max)\, p_{t}^{grid} \\ \text{s.t. (11), (14), (16), (18)-(20)} \end{cases} \tag{22}$$

Therefore, we can solve the single-level optimization problems ((21) and (22)) with off-the-shelf solvers instead of the previous hard-to-directly-solve bi-level optimization problem.

C. Acceleration Strategy

As introduced in Section II-B, the complementary slackness condition (17) is linearized by introducing a large constant M and binary variable θ_τ for each constraint. This transformation converts the bi-level optimization problems ((10)-(12) and (13)-(15)) into the single-level mixed-integer linear programming (MILP) problems ((21) and (22)). However, determining a suitable and safe value of the constant M for the traditional big-M method often requires considerable effort [5]. Moreover, an excessively large M usually makes the node relaxation over-loose, resulting in a larger number of nodes to be examined in the MILP solution process. To address these issues, we propose an enhanced big-M method in this subsection to enhance the computational efficiency of the MILP problem with the large constant M (i.e., (21) and (22)). The main idea involves independently evaluating a relatively tight M_τ for each constraint and replacing the traditional single safe M.

Firstly, randomly generate N_S wind power generation scenarios $\boldsymbol{P}_W^k$ $(k = 1, 2, \ldots, N_S)$ in the corresponding uncertainty set, based on which (8) and (9) are solved for the related primal optimal solutions $\{\boldsymbol{P}_G^{opt,k}, \boldsymbol{P}_{W,cur}^{opt,k}\}$ $(k = 1, 2, \ldots, N_S)$. Then, formulate and solve the following linear optimization problem for each wind power generation scenario.

$$\min \boldsymbol{1}^{\mathrm{T}}\boldsymbol{\lambda}^k \tag{23}$$

s.t.

$$\boldsymbol{\lambda}^k \ge \boldsymbol{0} \tag{24}$$

$$\mathrm{diag}(\boldsymbol{\lambda}^k)(\boldsymbol{E}\boldsymbol{P}_G^{opt,k} + \boldsymbol{F}\boldsymbol{P}_W^k + \boldsymbol{K}\boldsymbol{P}_{W,cur}^{opt,k} + \boldsymbol{G}) = \boldsymbol{0} \tag{25}$$

$$\begin{cases} 2\boldsymbol{A}\boldsymbol{P}_G^{opt,k} + \boldsymbol{B} + \boldsymbol{E}^{\mathrm{T}}\boldsymbol{\lambda}^k = \boldsymbol{0} \\ \boldsymbol{K}^{\mathrm{T}}\boldsymbol{\lambda}^k = \boldsymbol{0} \end{cases} \tag{26}$$

Constraints (24) and (25) guarantee the dual feasible and complementary slackness condition; and constraint (26) is the stationary condition. Since $\{\boldsymbol{P}_G^{opt,k}, \boldsymbol{P}_{W,cur}^{opt,k}\}$ is primal feasible, the solution $\boldsymbol{\lambda}^{opt,k}$ is dual optimal for $\boldsymbol{P}_W^k$.

Then, calculate $\lambda_\tau^{\max}$ and $\mu_\tau^{\max}$ as:

$$\lambda_\tau^{\max} = \max \lambda_\tau^{opt,k} \quad \forall k \tag{27}$$

$$\mu_\tau^{\max} = \max \left| \boldsymbol{E}_\tau \boldsymbol{P}_G^{opt,k} + \boldsymbol{F}_\tau \boldsymbol{P}_W^k + \boldsymbol{K}_\tau \boldsymbol{P}_{W,cur}^{opt,k} + \boldsymbol{G}_\tau \right| \quad \forall k \tag{28}$$

where $\boldsymbol{E}_\tau$, $\boldsymbol{F}_\tau$, $\boldsymbol{K}_\tau$, and $\boldsymbol{G}_\tau$ denote the τ^{th} rows of $\boldsymbol{E}$, $\boldsymbol{F}$, $\boldsymbol{K}$, and $\boldsymbol{G}$, respectviely.

Finally, we determine an M_τ for the τ^{th} constraint as:

$$M_\tau = \min\{\max\{\lambda_\tau^{\max}, \mu_\tau^{\max}\} \cdot m_1 + m_2, m_3\} \tag{30}$$

where m_1 is the reliability coefficient, which linearly enlarges $\max\{\lambda_\tau^{\max}, \mu_\tau^{\max}\}$ and usually takes 1.1-1.5; m_2 provides an offset, especially when $\max\{\lambda_\tau^{\max}, \mu_\tau^{\max}\}$ is 0, and usually takes multiples of the per-unit value, such as 10; and m_3 limits the maximum value of M_τ, which aims to prevent M_τ from being assigned an over-enlarged value and usually takes 10^5 - 10^6. By calculating M_τ as presented above, most of M_τ will be much smaller than the traditional safe M. When solving (21) and (22), we replace M with M_τ in the τ^{th} constraint, which tightens the node relaxation in the MILP solving process. This improvement can significantly improve the computational efficiency of EBC-EOR, which is detailedly verified in Section IV-E. It is worth mentioning that m_1, m_2, and m_3 cannot be set over-large, especially m_1. Otherwise, the computational efficiency will decline, even close to the traditional big-M method in the worst case. We suggest a parameter-setting strategy: try to increase the number of sampling scenarios N_S, and on this basis, choose relatively smaller values for m_1 and m_2, and a larger value for m_3 (usually the same as the safe M in the traditional big-M method).

IV. Illustrative Example

In this section, we conduct case studies on the modified IEEE 9-bus and IEEE 57-bus test systems. All the case studies are conducted on a computer equipped with a 2.80 GHz CPU and 16 GB RAM, utilizing Gurobi 10.0.1 under a Free Academic License.

A. System Description

To facilitate example design, we consistently set the total

scheduling time periods N_T to be 24 hours and assume that the load demand at each bus fluctuates proportionally. Appendix B presents the total load demand of the test systems at each time step. For the IEEE 9-bus test system, two wind farms are connected to buses 7 and 9, respectively, with their predicted output power indicated in Appendix B. The maximum and minimum output power of all generators is modified as 100 MW and 30 MW, respectively. The ramp-down/ramp-up limit of generators is set as 30 MW/h, and the rated transmission power of each branch is provided in Appendix C. For the IEEE 57-bus test system, two wind farms are connected to buses 8 and 12, respectively, with their corresponding predicted output power listed in Appendix A. The minimum output power of all generators is modified as 30% of their rated power, and the ramp-down/ramp-up limit is set as 100 MW/h. The rated transmission power of all branches is set as 200 MW.

B. Illustration Analysis of EBC-EOR

In this subsection, we visually compare the EBC-EOR, as defined in this paper, with the box-constrained operating region (BC-OR) formulated based on the two-stage robust optimization algorithm [29]. The BC-OR, as introduced in [29], involves setting the upper and lower bounds of the operating range of generators as decision variables in the master problem. In the subproblem, the upper and lower bounds of the operating range of generators are taken as known parameters, based on which the extreme scenario corresponding to the highest generation cost is solved. Subsequently, the extreme scenario is added to the master problem, and the master problem is solved again to update the upper and lower bounds. This iterative process continues until the termination condition is met, resulting in the final BC-OR.

For convenience, we assume the wind power generation uncertainty to be ±60% of the predicted value, based on which the BC-ORs and EBC-EORs of the generators and the power grid are calculated.

In Fig. 2, we visually compare the EBC-EOR with the BC-OR. The dark blue lines in Fig. 2(b) represent the OSP of generators adapted to the specific wind power generation scenario in Fig. 2(a). In Fig. 2(c), the dark blue line represents the corresponding OSP of power grid (sum of optimal output of all generators, not simply the sum of EBC-EORs of generators).

From Fig. 2(b) and (c), it is evident that the BC-OR fails to encompass the OSP corresponding to the output scenarios depicted in Fig. 2(a). However, this limitation is overcome by the EBC-EOR calculated using the proposed algorithm. The reason behind this disparity lies in the formulation of the BC-OR, which necessitates all operating points within the operating region of each adjacent time step to comply with the ramp-rate limits of generators [29], resulting in an inability to cover all the OSPs and exhibiting a conservative nature to a certain extent. In contrast, the EBC-EOR calculated using the proposed algorithm accurately delineates the economic operating boundary, encompassing all the OSPs and exhibiting superior economic performance.

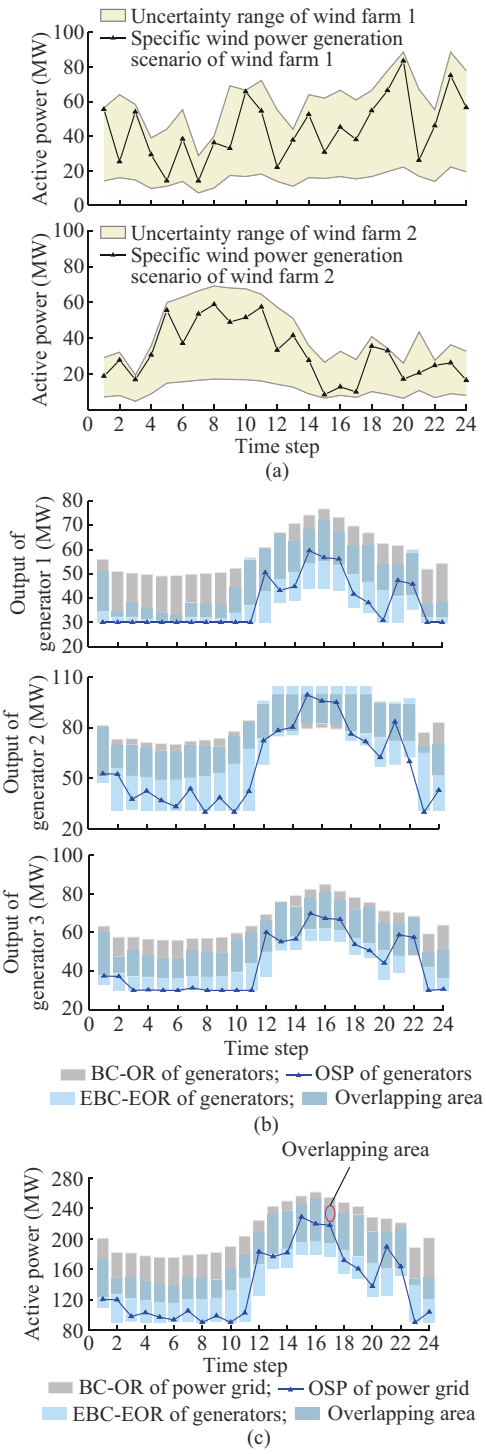

Fig. 2. Illustration analysis of EBC-EOR. (a) Wind power generation uncertainty. (b) BC-ORs and EBC-EORs of generators. (c) BC-ORs and EBC-EORs of power grid.

Besides, it is noticeable that the proposed EBC-EOR can be easily visualized regardless of the number of generators.

C. Economics Comparison of EBC-EOR

The visual analysis in the preceding section demonstrates that a specific wind power generation scenario can result in a corresponding OSP that falls outside the BC-OR but within the EBC-EOR. In this subsection, we further investigate

and compare the economics of the BC-OR and the EBC-EOR. First, we consider three kinds of wind power generation uncertainties: ±20%, ±40%, and ±60% of the predicted power, respectively. Next, we randomly generate 500 wind power generation scenarios from each uncertainty set. Finally, we calculate the general OSPs, the OSPs within the BC-OR, and the OSPs within the EBC-EOR based on the corresponding scenarios. The calculation results are presented in Table I.

TABLE I
ECONOMICS ANALYSIS

Wind power generation uncertainty (%)	Proportion of OSP not in BC-OR (%)	Proportion of OSP not in EBC-EOR (%)	Average generation cost within EBC-EOR (ratio to OSPs)	Average generation cost within BC-OR (ratio to OSPs)	The maximum ratio of generation cost within BC-OR to OSP
±20	54.2	0	$53561 (1.0000)	$53841 (1.0052)	1.0098
±40	99.6	0	$53710 (1.0000)	$54620 (1.0169)	1.0342
±60	100.0	0	$53959 (1.0000)	$56231 (1.0421)	1.0754

When the wind power generation uncertainty is ±20% of the predicted power, the average optimal operation cost within the BC-OR is 0.52% higher than that of the corresponding general OSPs. 54.2% of the scheduling plans in the BC-OR are not general OSPs, and the maximum ratio of the operation cost within the BC-OR to the related general OSP is 1.0098. As the wind power generation uncertainty increases to ±40% of the predicted power, the average optimal operation cost within the BC-OR is 1.69% higher than that of the corresponding general OSPs. Notably, 99.6% of the scheduling plans within the BC-OR are not general OSPs, and the maximum ratio of the operation cost within the BC-OR to the related general OSP is 1.0342. Furthermore, when the wind power generation uncertainty expands to ±60% of the predicted power, the average optimal operation cost within the BC-OR experiences a further increase to 4.21% higher than that of the corresponding general OSPs. In this case, none of the scheduling plans within the BC-OR align with the general OSPs, and the maximum ratio of the operation cost within the BC-OR to the related general OSP reaches 1.0754. The high proportion of scheduling plans within the BC-OR that do not match the general OSPs can be attributed to the requirement that the operating points within the BC-OR of adjacent time steps must satisfy the ramp-rate limits of generators. As a result, the scheduling plans within the BC-OR often fail to fully utilize the ramping ability of generators. This limitation becomes more pronounced as the wind power generation uncertainty increases, leading to a greater economic impact.

However, when considering the aforementioned three types of wind power generation uncertainty, the average operation cost of the scheduling plans within the EBC-EOR aligns with that of the general OSPs. Moreover, the proportion of OSPs not included in EBC-EOR is 0, indicating that the EBC-EOR successfully encompasses all general OSPs. By directing the operation of power grid based on EBC-EOR, superior economic performance can be achieved. Therefore, the proposed EBC-EOR is well-suited for the SACM.

D. Comparison with MPC

This subsection presents the relationship between the EBC-EOR of generator and MPC-based dispatching plans. For simplicity, we continue to utilize the modified IEEE 9-bus test system, employing the EBC-EOR and wind power output uncertainty sets from Section IV-B. We randomly sample 1000 wind power generation scenarios and calculate the MPC-based dispatching plans for different combinations of MPC prediction time periods H and MPC prediction errors. The simulation results of the simulations are summarized in Table II, where R1 represents the proportion of MPC-based dispatching plans falling within EBC-EOR, and R2 denotes the proportion of MPC-based dispatching plans resulting in load shedding.

TABLE II
SIMULATION RESULT WITH DIFFERENT H AND MPC PREDICTION ERRORS

MPC prediction error (%)	$H=2$		$H=4$	
	R1 (%)	R2 (%)	R1 (%)	R2 (%)
±20	64.0	2.5	65.0	2.3
±15	70.9	2.0	73.1	1.9
±10	77.9	1.7	78.7	1.5

As shown in Table II, it is observed that larger H and smaller MPC prediction error lead to a higher proportion of MPC-based dispatching plans falling within the EBC-EOR and a lower occurrence of load shedding. This can be attributed to the fact that the EBC-EOR fundamentally provides a spectrum of the global optimal dispatching plan set under uncertainties. Increasing the MPC prediction time periods and reducing the MPC prediction error can bring the MPC-based dispatching plan closer to the global optimum, thus increasing the likelihood of falling within the EBC-EOR. The occurrence of load shedding in the MPC-based dispatching plan is attributable to its typically shorter prediction time periods. In cases where the wind farm output power experiences significant fluctuations and the available reserve power is insufficient, load shedding is likely to occur due to the constraints imposed by the ramp-up/ramp-down capabilities of generators.

E. Computational Efficiency Comparison

This subsection compares the computational efficiency improvement of the proposed acceleration strategy (enhanced big-M method) with the traditional big-M method. We set

$M=10^5$ for the traditional big-M method and set $N_S=1000$, $m_1=1.5$, $m_2=10$, $m_3=10^5$ for the enhanced big-M method. Figure 3 shows the frequency counts of M_τ of the IEEE 9-bus and 57-bus test systems under different wind power generation uncertainties evaluated by the proposed acceleration strategy (enhanced big-M method). From Fig. 3, we can see that when the wind power generation uncertainty is slight, the value distribution of M_τ is relatively small. As the wind power generation uncertainty increases, the maximum value of M_τ also increases. For the IEEE 9-bus and 57-bus test systems, when the wind power generation uncertainty is ±60%, the maximum values of M_τ are 4532.40 and 19532.79, respectively. But only a small proportion of M_τ is relatively large. For the IEEE 9-bus test system, more than 82% of M_τ are within 100. For the IEEE 57-bus test system, more than 94% of M_τ are within 400. Compared with the traditional big-M method, the proposed enhanced big-M method can adaptively evaluate M_τ for each constraint and decrease M_τ significantly. Thus, the acceleration strategy can alleviate the problem of excessive node relaxation in formulating the EBC-EOR (solving MILP repeatedly) caused by the traditional big-M method.

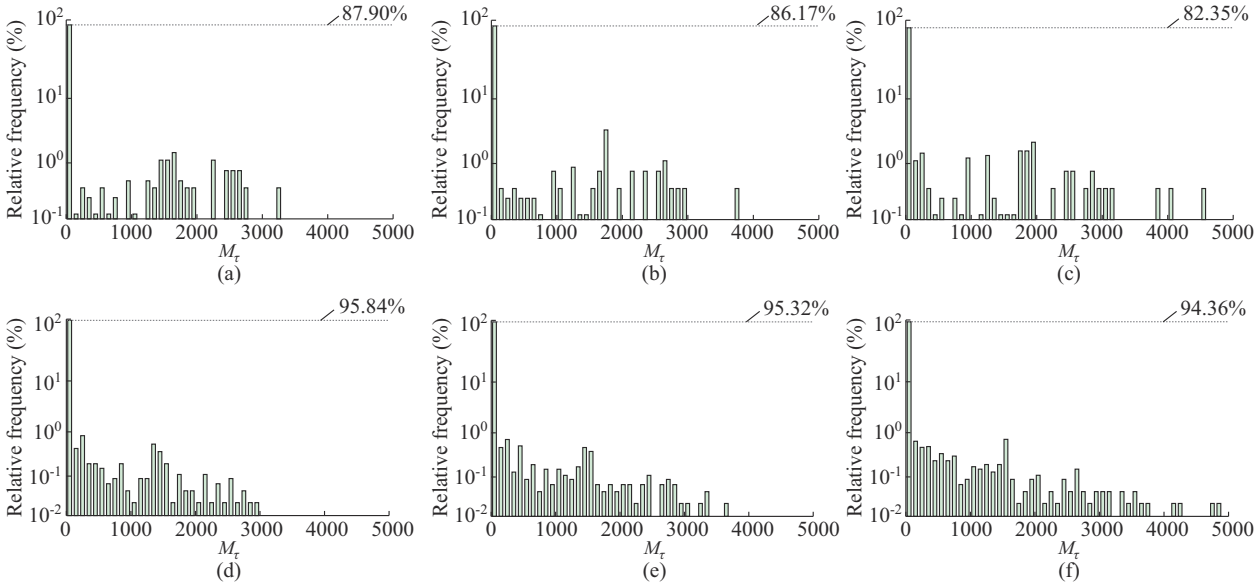

Fig. 3. Frequency counts of M_τ. (a) IEEE 9-bus test system (wind power generation uncertainty is ±20%). (b) IEEE 9-bus test system (wind power generation uncertainty is ±40%). (c) IEEE 9-bus test system (wind power generation uncertainty is ±60%). (d) IEEE 57-bus test system (wind power generation uncertainty is ±20%). (e) IEEE 57-bus test system (wind power generation uncertainty is ±40%). (f) IEEE 57-bus test system (wind power generation uncertainty is ±60%).

Table III shows the computational time of the EBC-EOR for the IEEE 9-bus and IEEE 57-bus test systems with the traditional and enhanced big-M methods.

TABLE III
COMPARISON OF COMPUTATIONAL TIME OF EBC-EOR

Test system	Wind power generation uncertainty (%)	Computational time (s)	
		Traditional big-M method	Enhanced big-M method
IEEE 9-bus	±20	755.55	2.70
	±40	735.45	3.35
	±60	>900	6.64
IEEE 57-bus	±20	>900	25.74
	±40	>900	37.34
	±60	>900	72.60

The traditional big-M method takes more than 700 s for the IEEE 9-bus test system and more than 900 s for the IEEE 57-bus test system. However, after applying the proposed acceleration strategy (enhanced big-M method), it takes less than 7 s for the IEEE 9-bus test system and less than 75 s for the IEEE 57-bus test system. According to Table III, the proposed big-M method can significantly improve the efficiency of the traditional big-M method in formulating the EBC-EOR at least twelvefold.

V. CONCLUSION

This paper presents a mathematical definition of the EBC-EOR for both the power grid and its dispatchable components. We introduce bi-level optimization models and a solution algorithm to determine the EBC-EOR. Additionally, an acceleration strategy (enhanced big-M method) is proposed to enhance computational efficiency. Through case studies conducted on two test systems, we demonstrate that the EBC-EOR can encompass 100% of the general OSPs of power grid, and the acceleration strategy can reduce computaional time by more than twelvefold. The EBC-EOR can be formulated offline and implemented online to assess the economic operation of the power grid. Moreover, when combined with the online OSP matching algorithm, it serves as a critical technology to support the steady-state adaptive cruise of power grid.

In our future work, we plan to extend the EBC-EOR formulation to consider unit commitment and energy storage (both power-side and grid-side). We will develop a corre-

sponding online OSP fast-matching algorithm for efficient implementation. Additionally, we aim to explore the application of the EBC-EOR in the context of the electricity market.

APPENDIX A

To help understand the specific elements and connotations of the coefficient matrices and vectors in the compact-form scheduling model, we take the modified "case4gs" test system in Matpower 7.1 [35] as an example and provide the specific composition of the relevant coefficient matrices and vectors. Let the number of scheduling time periods $N_T=2$. The maximum and minimum output power of generators is set to be 200 MW and 30 MW, respectively. The ramp-up and ramp-down rates of generator are all set to be 60 MW/h. Let $a_1=0.11$, $b_1=5$, $c_1=150$, $a_2=0.085$, $b_2=1.2$, and $c_2=600$. A wind farm is connected at bus 2, and the predicted power of the wind farm at $t=1$ and $t=2$ is 66 MW and 75 MW, respectively. The grid load at $t=1$ and $t=2$ is 378.00 MW and 406.35 MW, respectively.

Since the decision variable vectors influence the coefficient matrices and vectors, we first set $\boldsymbol{P}_G$, $\boldsymbol{P}_W$, and $\boldsymbol{P}_{W,cur}$ as:

$$\boldsymbol{P}_G=\begin{bmatrix} p_{1,1}^{G} \\ p_{2,1}^{G} \\ p_{1,2}^{G} \\ p_{2,2}^{G} \end{bmatrix} \tag{A1}$$

$$\boldsymbol{P}_W=\begin{bmatrix} p_{1,1}^{W} \\ p_{1,2}^{W} \end{bmatrix} \tag{A2}$$

$$\boldsymbol{P}_{W,cur}=\begin{bmatrix} p_{1,1}^{W,cur} \\ p_{1,2}^{W,cur} \end{bmatrix} \tag{A3}$$

Then, we calculate the power transfer distribution factor (PTDF) matrix of the test system (with bus 1 as the slack bus) as follows, which can be conveniently calculated using Matpower [35].

$$\boldsymbol{PTDF}=\begin{bmatrix} 0 & -0.7325 & -0.1975 & -0.5350 \\ 0 & -0.2675 & -0.8025 & -0.4650 \\ 0 & 0.2675 & -0.1975 & -0.5350 \\ 0 & -0.2675 & 0.1975 & -0.4650 \end{bmatrix} \tag{A4}$$

Finally, construct the coefficient matrices $\boldsymbol{A},\boldsymbol{E},\boldsymbol{F},\boldsymbol{K}$ and the coefficient vectors $\boldsymbol{B},\boldsymbol{C},\boldsymbol{G}$, of which the expressions are given in the Supplementary Material. The elements of $\boldsymbol{A}$, $\boldsymbol{B}$, and $\boldsymbol{C}$ are mainly composed of the cost coefficients of the generators. In $\boldsymbol{E}$, $\boldsymbol{F}$, $\boldsymbol{K}$, and $\boldsymbol{G}$, the first to the fourth rows represent the minimum output power constraints of the generators; the fourth to the eighth rows represent the maximum output power constraints of the generators; the ninth and tenth rows represent the ramp-up constraints of the generators; the eleventh and twelfth rows represent the ramp-down constraints of the generators; the thirteenth to the twenty-eighth rows represent the power flow constraints; the twenty-ninth to the thirty-second rows represent the power balance constraints; and the thirty-third to thirty-sixth rows represent the wind curtailment power constraints.

APPENDIX B

TABLE BI
LOAD LEVEL AND PREDICTED WIND POWER GENERATION

Time	IEEE 9-bus			IEEE 57-bus		
	Load level (MW)	Predicted wind generation (MW)		Load level (MW)	Predicted wind generation (MW)	
		Wind farm 1	Wind farm 2		Wind farm 1	Wind farm 2
1	194.48	35.20	18.24	1240.54	100.00	57.61
2	172.65	40.00	20.16	1100.20	125.00	63.43
3	168.68	36.48	12.16	1073.44	114.13	38.22
4	162.73	24.32	22.40	1036.04	76.09	70.60
5	166.70	27.52	37.44	1089.45	86.96	117.63
6	168.68	34.56	39.36	1082.19	108.70	123.63
7	172.65	17.92	41.60	1100.20	56.52	132.40
8	174.64	24.96	43.20	1102.96	78.26	135.42
9	180.59	43.20	42.56	1140.35	135.87	133.84
10	194.48	41.60	42.24	1228.79	130.43	132.46
11	214.33	45.12	40.32	1354.12	141.30	126.41
12	238.14	34.56	35.84	1504.84	108.70	112.01
13	256.00	27.52	32.00	1617.53	86.96	100.20
14	261.95	40.00	22.40	1655.56	125.10	70.62
15	267.91	38.72	16.64	1692.96	121.74	52.81
16	277.83	41.60	20.48	1730.36	130.43	64.01
17	265.92	38.08	17.60	1668.07	119.57	55.26
18	261.95	41.60	25.60	1656.81	130.33	80.88
19	259.97	48.64	21.44	1643.05	152.17	67.80
20	238.14	55.36	16.32	1504.84	173.91	51.61
21	236.16	41.92	27.20	1492.45	131.43	85.80
22	234.17	34.56	17.28	1486.08	108.87	54.42
23	178.61	55.36	22.72	1128.60	173.91	71.61
24	176.62	48.64	20.48	1115.46	152.17	64.60

APPENDIX C

TABLE CI
RATED TRANSMISSION POWER OF BRANCHES IN IEEE 9-BUS TEST SYSTEM

Branch No.	Rated transmission power (MW)
1-4	170
4-5	80
5-6	70
3-6	170
6-7	70
7-8	170
8-2	170
8-9	100
9-4	70

REFERENCES

[1] Y. Dong, X. Shan, Y. Yan *et al*., "Architecture, key technologies and applications of load dispatching in china power grid," *Journal of Modern Power Systems and Clean Energy*, vol. 10, no. 2, pp. 316-327, Mar. 2022.

[2] White House. (2021, Jan.) Executive order on tackling the climate crisis at home and abroad. [Online]. Available: https://www.energy.gov/nepa/articles/eo-14008-tackling-climate-crisis-home-and-abroad-2021

[3] J. Xi, "Statement at the general debate of the 75th session of the united nations general assembly," *Gazette of the State Council of the People's Republic of China*, vol. 28, pp. 5-7, Sept. 2020.
[4] A. S. A. Awad, D. Turcotte, and T. H. M. El-Fouly, "Impact assessment and mitigation techniques for high penetration levels of renewable energy sources in distribution networks: voltage-control perspective," *Journal of Modern Power Systems and Clean Energy*, vol. 10, no. 2, pp. 450-458, Mar. 2022.
[5] W. Wei, F. Liu, and S. Mei, "Dispatchable region of the variable wind generation," *IEEE Transactions on Power Systems*, vol. 30, no. 5, pp. 2755-2765, Sept. 2015.
[6] W. Wei, F. Liu, and S. Mei, "Real-time dispatchability of bulk power systems with volatile renewable generations," *IEEE Transactions on Sustainable Energy*, vol. 6, no. 3, pp. 738-747, Jul. 2015.
[7] B. Hu and L. Wu, "Robust SCUC considering continuous/discrete uncertainties and quick-start units: a two-stage robust optimization with mixed-integer recourse," *IEEE Transactions on Power Systems*, vol. 31, no. 2, pp. 1407-1419, Mar. 2016.
[8] C. Wang, F. Liu, J. Wang *et al*., "Risk-based admissibility assessment of wind generation integrated into a bulk power system," *IEEE Transactions on Sustainable Energy*, vol. 7, no. 1, pp. 325-336, Jan. 2016.
[9] H. Haghighat and B. Zeng, "Stochastic and chance-constrained conic distribution system expansion planning using bilinear Benders decomposition," *IEEE Transactions on Power Systems*, vol. 33, no. 3, May 2018.
[10] P. Li, D. Yu, M. Yang *et al*., "Flexible look-ahead dispatch realized by robust optimization considering CVaR of wind power," *IEEE Transactions on Power Systems*, vol. 33, no. 5, pp. 5330-5340, Sept. 2018.
[11] X. Lu, K. W. Chan, S. Xia *et al*., "Security-constrained multiperiod economic dispatch with renewable energy utilizing distributionally robust optimization," *IEEE Transactions on Sustainable Energy*, vol. 10, no. 2, pp. 768-779, Apr. 2019.
[12] Y. Shi, S. Dong, C. Guo *et al*., "Enhancing the flexibility of storage integrated power system by multi-stage robust dispatch," *IEEE Transactions on Power Systems*, vol. 36, no. 3, pp. 2314-2322, May 2021.
[13] J. Guan, H. Tang, K. Wang *et al*., "A parallel multiscenario learning method for near-real-time power dispatch optimization," *Energy*, vol. 202, p. 117708, Jul. 2020.
[14] J. Guan, H. Tang, J. Wang *et al*., "A gan based fully model-free learning method for short-term scheduling of large power system," *IEEE Transactions on Power Systems*, vol. 37, no. 4, pp. 2655-2665, Jul. 2022.
[15] H. Xu, J. Yao, G. Nan *et al*., "New features of application function for future dispatching and control systems," *Automation of Electric Power Systems*, vol. 42, no. 1, pp. 1-7, Jan. 2018.
[16] J. Yao, K. Wang, D. Xu *et al*., "Architecture of steady-state adaptive cruise scenario for large-scale power grid dispatching," *Automation of Electric Power Systems*, vol. 43, no. 22, pp. 179-186, Nov. 2019.
[17] H. Xu, J. Yao, Y. Yu *et al*., "Architecture and key technologies of dispatch and control system supporting integrated bulk power grids," *Automation of Electric Power Systems*, vol. 42, no. 6, pp. 1-8, Mar. 2018.
[18] J. Zhao, Y. Zhang, D. Su *et al*., "Architecture and key technologies of automatic cruise for AC/DC bulk power grid dispatching," *Automation of Electric Power Systems*, vol. 43, no. 22, pp. 187-193, Nov. 2019.
[19] J. Xiao, W. Gu, C. Wang *et al*., "Distribution system security region: definition, model and security assessment," *IET Generation, Transmission & Distribution*, vol. 6, no. 10, pp. 1029-1035, Oct. 2012.
[20] J. Xiao, G. Zu, X. Gong *et al*., "Model and topological characteristics of power distribution system security region," *Journal of Applied Mathematics*, vol. 2014, Jul. 2014.
[21] J. Xiao, G. Zu, X. Gong *et al*., "Observation of security region boundary for smart distribution grid," *IEEE Transactions on Smart Grid*, vol. 8, no. 4, pp. 1731-1738, Jul. 2017.
[22] G. Zu, J. Xiao, and K. Sun, "Mathematical base and deduction of security region for distribution systems with DER," *IEEE Transactions on Smart Grid*, vol. 10, no. 3, pp. 2892-2903, May 2019.
[23] J. Xiao, G. Zu, Y. Wang *et al*. "Model and observation of dispatchable region for flexible distribution network," *Applied Energy*, vol. 261, p. 114425, Mar. 2020.
[24] S. Chen, Z. Wei, G. Sun *et al*. "Convex hull based robust security region for electricity-gas integrated energy systems," *IEEE Transactions on Power Systems*, vol. 34, no. 3, pp. 1740-1748, May 2019.
[25] T. Jiang, R. Zhang, X. Li *et al*., "Integrated energy system security region: concepts, methods, and implementations," *Applied Energy*, vol. 283, p. 116124, Feb. 2021.
[26] W. Lin, Z. Yang, J. Yu *et al*., "Tie-line security region considering time coupling," *IEEE Transactions on Power Systems*, vol. 36, no. 2, pp. 1274-1284, Mar. 2021.
[27] Y. Zhang, J. Zhao, Z. Liu *et al*., "Construction method of economic operation region in automatic cruise for bulk power grid dispatching," *Automation of Electric Power Systems*, vol. 44, no. 12, pp. 64-73, Jun. 2020.
[28] Y. Shi, "Multi-stage robust dispatch of power system considering uncertainties of renewable energy," Ph.D. dissertation, Zhejiang University, Hangzhou, China, 2021.
[29] Y. Cho, T. Ishizaki, N. Ramdani *et al*., "Box-based temporal decomposition of multi-period economic dispatch for two-stage robust unit commitment," *IEEE Transactions on Power Systems*, vol. 34, no. 4, pp. 3109-3118, Jul. 2019.
[30] H. Xu, B. Jiang, B. Feng *et al*., "The concept of economy operation region and its convex hull solution method for quantifying the influence of grid uncertainty on scheduling plan," *Proceedings of CSEE*, doi: 10.13334/j.0258-8013.pcsee.220360
[31] Z. Tan, H. Zhong, Q. Xia *et al*., "Estimating the robust *P-Q* capability of a technical virtual power plant under uncertainties," *IEEE Transactions on Power Systems*, vol. 35, no. 6, pp. 4285-4296, Nov. 2020.
[32] S. Boyd and L. Vandenberghe, "Duality," in *Convex Optimization*, 1st ed., Cambridge: Cambridge University, 2004, pp. 215-271.
[33] P. Yang and A. Nehorai, "Joint optimization of hybrid energy storage and generation capacity with renewable energy," *IEEE Transactions on Smart Grid*, vol. 5, no. 4, pp. 1566-1574, Jul. 2014.
[34] Z. Chen, Z. Li, C. Guo *et al*., "Fully distributed robust reserve scheduling for coupled transmission and distribution systems," *IEEE Transactions on Power Systems*, vol. 36, no. 1, pp. 169-182, Jan. 2021.
[35] R. D. Zimmerman and C. E. Murillo-Sanchez. (2020, Dec.). Matpower (Version 7.1). [Online]. Available: https://matpower.org

Huating Xu received the B.S. degree from Sichuan University, Chengdu, China, in 2012, and the M.S. degree from China Electric Power Research Institute, Beijing, China, in 2020. Presently, he is working toward the Ph.D. degree with the College of Electrical Engineering, Zhejiang University, Hangzhou, China. He was an Electrical Engineer with the China General Nuclear Power Group, Dalian, China, from 2012 to 2017. His current research interests include deep reinforcement learning, reactive power and tie-line power adjustment, optimal power flow, and economic dispatching region.

Bin Feng received the B.S. degree in electrical engineering and its automation from the North Chine Electric Power University, Beijing, China, in 2019. He is presently working towards the Ph.D. degree in Zhejiang University, Hangzhou, China. His current research interests include deep reinforcement learning, federated learning, energy management, and forecasting.

Chutong Wang is currently working towards the Ph. D. degree in the School of Electrical Engineering, Zhejiang University, Hangzhou, China. His research interests include integrated energy system planning, energy storage system configuration, and shared energy storage.

Chuangxin Guo received the Ph. D. degree in electrical engineering from Huazhong University of Science and Technology, Wuhan, China, in 1997. He is currently a Professor with the College of Electrical Engineering, Zhejiang University, Hangzhou, China. His research interests include power system operation and planning, and power system information and communication technologies.

Jian Qiu received the Ph.D. degree in electrical engineering from Zhejiang University, Hangzhou, China, in 2016. He is currently a Researcher with the College of Electrical Engineering, Zhejiang University. His research interests include big data, artificial intelligence (AI), and application of digital twin technique in power system.

Mingyang Sun received the Ph.D. degree from the Department of Electrical and Electronic Engineering, Imperial College London, London, U. K., in 2017. From 2017 to 2019, he was a Research Associate and a DSI Affiliate Fellow with Imperial College London. He is currently a Professor of control science and engineering under the Hundred Talents Program with Zhejiang University, Hangzhou, China. He is also an Honorary Lecturer with Imperial College London. His research interests include AI in energy systems and cyber-physical energy system security and control.